CrossMark

# Numerical and Experimental Investigation of the Hydrostatic Performance of Fibre Reinforced Tubes

**S. Pavlopoulou**[1] ⓘ **· S. S. Roy**[1] **· M. Gautam**[1] **·
L. Bradshaw**[1] **· P. Potluri**[1]

**Abstract** The increasing demands in subsea industry such as oil and gas, led to a rapidly growing need for the use of advanced, high performance, lightweight materials such as composite materials. E-glass fibre laminated pre-preg, filament wound and braided tubes were tested to destruction under hydrostatic external pressure in order to study their buckling and crushing behaviour. Different fibre architectures and wind angles were tested at a range of wall thicknesses highlighting the advantage that hoop reinforcement offers. The experimental results were compared with theoretical predictions obtained from classic laminate theory and finite element analysis (ABAQUS) based on the principal that the predominant failure mode was buckling. SEM analysis was further performed to investigate the resulting failure mechanisms, indicating that the failure mechanisms can be more complex with a variety of observed modes taking place such as fibre fracture, delamination and fibre-matrix interface failure.

**Keywords** Filament winding · Braiding · Buckling analysis · Hydrostatic external pressure · Textile composites

## 1 Introduction

As the requirement for achieving higher subsea depths is increasing so does the demand for the use of lightweight, high performance composite materials, in an effort to replace the

✉ S. Pavlopoulou
sofia.pavlopoulou@gmail.com

S. S. Roy
shankhachur.roy@manchester.ac.uk

1    School of Materials, University of Manchester, Oxford Road, Manchester,
M13 9PL, UK

traditionally employed metallic structures. The move towards exploration and development of composite materials for deep-water subsea applications in oil and gas industry, can minimise the structural weight which can be difficult and costly to accommodate at high water depths. In addition, the remarkably high properties and strength of composite materials can offer a structural alternative for the design of a number of structures such as drill risers.

There has been a recent interest in utilising weaving techniques from the textiles industry in order to produce high performance fabrics for composite structures. These manufacturing techniques aim to overcome problems related to laminated composites, such as delaminations and interface mismatch between the constituent materials through the interlacing of the tows in the through-thickness direction [1]. More specifically braiding technology has been suggested for a number of commercial applications such as fuel lines, rocket launch tubes and aircraft structural parts due to the structural advantage over alternative weaving techniques. Three of its major competitors are filament winding, pultrusion and tape lay-up.

Several studies have drawn the attention on the advantages of braiding in terms of structural integrity, design flexibility, damage tolerance, repair ability and low manufacturing cost [2]. Complex shapes can be easily produced while the performance can be controlled through the regulation of the braid, crimp angle and other geometrical characteristics. Braided tubes exhibit a superior structural strength due to the fact that the interlacements act as crack arrests in contrast to laminated and filament wound tubes where the cracks run along the fibres [3, 4].

Several studies have focused on the crush behaviour of laminated, woven and knitted composite tubes. These studies investigated the parameters that can affect the crushing characteristics such as fibre and matrix materials, fibre pattern and shell geometry. In addition extensive work has been carried out on the numerical analysis and investigation of the crushing modes. However little work has focused on the energy absorption and crushing mode analysis of braided tubes. Among the most notable work; Karbhari et al. highlighted the advantages of 2D braided composite tubes for energy absorption applications by studying different types of fibres, numbers of layers and braid patterns [5]. Chiu et al. concluded that braided composite tubes with 20° angle exhibited advanced energy absorption performance [6]. Chiu et al. studied the use of hybrid 2D braided composite tubes reinforced with Kevlar and carbon fibres and identified their crushing modes [7].

The current research aims to add to the existing knowledge starting from the more conventional laminated (tape layup) tubes, and then expanding to filament wound and braided tubes, all reinforced with E-glass fibres. This was achieved through the experimental testing of samples at a range of wall thickness and reinforcement angles and through the understanding of their complex failure mechanisms when subjected to hydrostatic external loads. This work also studied the optimum fibre angle that can provide higher performance under externally applied pressure. The outcome was further correlated with the traditionally employed netting analysis according to which the optimum angle is 55°. To enable the optimisation study, finite element models were developed for each fibre reinforced tube category which were further validated with experimental results.

In Section 2, a brief review of filament winding and braiding methods is presented, focusing on manufacturing and geometrical aspects of composite tubes. In Section 3 details regarding the mechanisms and investigation of externally pressurised composite tubes are discussed referring to previous work. In Section 4, the detailed experimental set up followed in the current work is displayed. Section 5 displays all the results obtained from experimental and numerical work. Finally Section 6 presents some concluding remarks.

## 2 Review of Filament Winding and Braiding for the Manufacturing of Composite Tubes

### 2.1 Filament Winding

Filament winding is one of the oldest manufacturing methods for composite manufacturing. The method is only used for non-interlaced fibre layup. The manufacturing process comprises of a rotating and a traversing unit. This simple mechanical processing allows winding filaments from helical to hoop orientation. The versatility in fibre layup at various angles and the simplicity of the mechanism made filament winding one of the widely used processes. The use of filament winding for composite manufacturing ranged from military to commercial uses in aerospace to hydrospace industries. Although filament winding can be used for developing structures such as wind turbines and engine fan blades, it is also widely used for manufacturing of a range of cylindrical structures. The method is extensively used for manufacturing composite pressure vessels, storage tanks, tubes and also solid rods.

Commercially available filament winding machines include a resin bath for impregnating the filaments before winding onto a rotating mandrel. The in-line wetting process eliminates the additional process of resin impregnation for a dry fibre preform. The traversing of the fibre delivery point along the length of the rotating mandrel produces a winding pattern widely known as hoop and helical winding. Winding angle is one of the major structural design parameters. During winding process the multiple layers are stacked on top of each other as the diameter changes in order to keep the desired winding angle relatively consistent between the layers, the process parameters-rotational and traverse speed requires adjusting. Experimental results from a previous study shows that winding angles $\pm 55°$ and $\pm 75°$ are optimum for biaxial and hoop pressure loading respectively [8]. Another study presented that for pure circumferential loading winding angle of $\pm 75°$ and for axial loading winding angle less than $\pm 55°$ exhibited higher stress at fracture [9]. It is evident that deciding optimum winding angle is required based on the composite application in consideration.

There are other processing parameters which can effect the performance of a filament wound composite structure and winding tension is one of those. The fibre tows are wound at high tension to achieve a consolidated structure. The desired fibre tension can be achieved from a tensioning device between the fibre delivery creel and the resin bath. A previous study suggests that an increased winding tension can aid to reach local fibre volume fraction as high as 70 % [10]. Higher winding tension also contributes to the mechanical properties for fibre dominated loading. An improved burst pressure and hoop modulus of composite cylinders was observed from the experiments in which higher winding tension was used [11].

Winding stacking sequence was observed to have influenced interlaminar shear properties [11]. A dispersed stacking of winding pattern achieved higher shear failure load compared to that of an aggregated stacking of the same pattern within the stack [11]. A few studies were also carried out on multi angle filament wound composites through the investigation of their thickness and stacking sequence [12, 13]. Higher winding angle in composite leads to higher hoop modulus that can resist buckling caused by external pressure whereas lower winding angle such as 20°, would contribute to higher axial modulus and strength. Hence multi axial filament winding exhibited to have improved tension and buckling properties [12].

## 2.2 Braiding

Braiding is a competing method to filament winding for developing cylindrical composites [14]. The principle of both techniques inherently produces cylindrical structures making them a good choice for manufacturing tubes. Both processes host the advantage of reinforcement continuity [9]. The method in which the fibre tows are laid onto mandrel by braiding is different than that of filament winding. This difference produces a bidirectional preform (+ve and −ve fibre orientation) in a single layer unlike filament winding. In addition, braid structure has fibre interlacement unlike filament winding. Finally there are differences in capabilities of fibre orientation in both techniques [14]. Compared with filament winding, braiding is a new technology within the preforming industry, for this reason research into braiding under external pressure conditions has been limited. There is therefore requirement for investigation into comparative analysis of composite tube under external pressure developed using braiding as well as filament winding and woven fabric wrapping.

### 2.2.1 Braiding Principle

The most common 2D braiding machines used for developing tubular preforms are either radial or maypole braiders. Both of these machines produce tubular braided preform with two sets of counter rotating bobbins with fibres. In order to produce a tubular braided preform of certain diameter, a solid core mandrel is used for over-braiding. The mandrel is mounted on a linear take up mechanism. In this study tubular mandrels were overbraided on a 48 carrier maypole braiding machine for producing composite tubes for hydrostatic performance evaluation.

During the bobbin rotation, as the carriers are mounted on horn gears, the counter-rotating fibres produce interlacement in helical orientation within the braid structure. For a braided structure the fibre orientation with respect to the mandrel axis is known as "braid angle". As the composite tube structural properties depend on fibre orientation, the angle can be manipulated by changing the rotational speed or linear take up speed for a given diameter of the mandrel.

Uniform take up is critical to the braid architecture; temporary increased take up (jerks) or pauses will produce respective localised braid extension or crowding [15]. Both of these occurrences will cause variations in braid angle. Rawal et al. identify four braid formation variables which combine to define a braided structure consisting of; the carrier speed about the braid deck (angular velocity), the take up speed, the mandrel cross-section and the number of yarns used [16].

### 2.2.2 Braid Architecture

Braid architecture can be explained with several parameters that specify the construction of the braid. These parameters are braid angle, cover factor and crimp which will eventually influence the mechanical properties of a braided composite. As explained in the previous section, braid angle is the magnitude of an off-axis position of a fibre located in the form of a helix within the braid. Once the fibre orientations are decided, prior to the braiding the angle ($\alpha$) can be calculated by using the following equation.

$$\alpha = tan^{-1}(\frac{\omega R}{v}) \tag{1}$$

where $\omega$ is the average angular velocity of bobbins (rad/s), $R$ is the radius of cylindrical mandrel (mm) and $v$ is the take up speed (mm/s).

Another important parameter is the cover factor which indicates the extent of mandrel surface coverage by the braid. If the surface is not fully covered, even with a multi layer braided preform, the uncovered areas can leave through the thickness resin pocket within the composite. The cover factor (*CF*) can be calculated using the following equation.

$$CF = 1 - (1 - \frac{W_y N_c}{4\pi R(cos\alpha)})^2 \tag{2}$$

In the above equation, $W_y$, $N_c$, $R$ and $\alpha$ indicate the fibre tow width, number of carriers, effective braid radius and braid angle respectively.

The crimp of the fibre tow within a braid structure is a measure of undulation due to the interlacement. In this study, all the braided preforms had a regular (2/2) pattern. The percentage of crimp (e) can be calculated considering the fibre interlacement (Fig. 1) which is used later in the study for finite element analysis.

$$e = \frac{L - l}{l} \cdot 100 \tag{3}$$

### 2.2.3 Braided Composites

Braiding is a textile preforming technique that offers increased transverse moduli, transverse strength, damage tolerance, dimensional stability and near net shape manufacturing capabilities [17]. Composites produced using the braiding technique exhibit superior strength and crack resistance to broadcloth composites [4]. Braided composites are also known to greatly improve interlaminar shear properties and depict no delamination as observed when braided composites are subjected to fatigue loadings [18].

Under uniaxial static load, an increase in braid angle leads to a decrease in the longitudinal modulus and an increase in transverse modulus. In addition, the shear modulus and the in-plane Poisson's ratio increase with an increase in braid angle with a maximum peak at ±45° [19]. The transverse moduli, strength, and dimensional stability of braided composites arise from helical fibres and the damage tolerance results from the locking mechanism between the intertwined fibres of the braid architecture that helps in preventing or limiting the yarn delamination [2].

Braided composites are known to have high specific energy absorption for tubular sections upon axial crushing when compared with metals [20]. The effect of braid angle upon energy absorption properties has been the focus of previous research which concluded that among 30°, 45° and 60° braiding angles, 60° is the braiding angle at which biaxially braided carbon fibre tubes exhibit highest specific energy absorption [21]. The effect of braid angle and axial tow insertion has also been investigated in previous work which reported that the braid angle of 20° results in the highest specific energy absorption [6]. Biaxial and triaxial braided composites with the same fibre-volume fractions have been compared with biaxial braided composites depicting higher peak load failing in ring-type crushing whilst the triaxial braided composites failing in a lamina bending mode [22]. Braided composites are
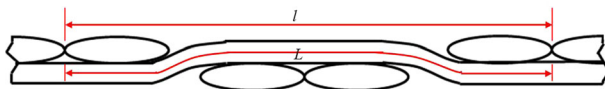


**Fig. 1** Side view of a braided textile illustrating measurements for crimp calculation notation

also known to exhibit high energy absorption under tensile mode with axial strain to failure values exceeding more than 60 % for a 55° braid angle for a single layer tubular braided composite [23].

# 3 Externally Pressurised Composite Tubes

The considerable extension of composite tubes to several applications in offshore engineering has increased the demand for externally pressurised composite tubes on top of internally pressurised. Pipes and vessels that are subject to pressure (internal or external) are subject to a combination of axial and hoop stresses, in certain mechanisms whose interaction is important to understand before design. The hoop and axial stresses exerted across the 2D plane of a cylinder wall are illustrated in Eqs. 4 and 5, which indicate that the hoop stress is twice that of the axial stress for a closed-end thin walled tube [24].

$$Hoop\ stress:\quad \sigma_H = \frac{P \cdot r}{t} \tag{4}$$

$$Axial\ stress:\quad \sigma_A = \frac{P \cdot r}{2t} \tag{5}$$

where $P$ is the applied pressure, $r$ is the radius of the tube and $t$ is the tube thickness.

However the underlying mechanisms for isotropic tubes are very different to the ones for anisotropic tubes. Netting analysis is one of the simplest methods that has been extensively used to identify the optimum reinforcement angle for fibre reinforced composite materials, particularly well suited to pressure vessels and tubes. This is a modelling technique which assumes that all loads are carried by the fibers only and the matrix strength and stiffness is taken to be negligible [25]. It also assumes that no shear loading is present resulting in a system where filaments are loaded with pure tensile or compressive stresses allowing for simplified analysis [26]. Equation 6 can therefore be derived, which describes the optimum reinforcement angle ($\alpha$) for cylinders and pipes under pressure loads [25]:

$$\alpha = tan^{-1}\sqrt{R} \tag{6}$$

where $R$ is the hoop to axial stress ratio ($\sigma_H/\sigma_A$). If we consider that the ratio $R$ is equal to 2, then the optimum angle is $\alpha$=54.73° for tubes under pure pressure loads [25].

A number of researchers have investigated the accuracy of netting analysis [26, 27] or used it as a base assumption for further work [25, 28]. Netting analysis provides a basis for the understanding and further analysis of the complex mechanisms that take place during failure when a composite tube reinforced with long fibres is subject to crushing loads. However the nature of these phenomena is expected to be more complicated, and the response depends on interaction between the different mechanisms that control the crushing process such as transverse shearing, lamina bending, and local buckling. These failure modes further depend on the mechanical properties of the constituent materials, the structure of the specimen, the crushing speed and the crushing length [29].

Some studies have previously suggested that although $\alpha$=55° offers the highest resistance to internal pressure, the same principle does not apply for buckling under external pressure [30]. The benefits of the extra reinforcement of the hoop direction were highlighted

first by Mistry [31] and later by Messeger et al. [32] who proved composite wound tubes consisting of high angle (80° and 90°) layers provided higher resistance to buckling under external pressure than $\alpha = 55°$. Several researchers have explored fracture phenomena, design parameters and failure modes of composite tubes under external loading or biaxial loading [33–35]. The fracture mechanisms can be very complex, resulting from a combination of different failure modes. Harte et al. found that the dominant failure mode of composite braided tubes subjected to compressive loads is diamond shaped buckling, which initiates at a peak stress and further propagates at a lower load as seen in Fig. 2a [36]. The work by Davies et al. which focused on the collapse failure mode of a hybrid steel/composite cylinder under hydrostatic pressure demonstrated that an out of plane lateral buckling was observed which was not predicted by the FE model [37]. In addition little work has focused on the understanding of how the fibre angle can influence the failure modes.

## 4 Specimen Preparation and Experimental Set Up

Tubes made of different manufacturing methods (laminated pre-preg, filament winding and braiding) were tested in this study. However the specimen preparation and testing method remained consistent to allow for a comparative investigation. The steps followed for the preparation of the specimens prior to testing are summarised below:

1. The supplied tubes were machined to the desired lengths; 220 mm length each.
2. Aluminium end caps were machined for push fit connections into the tube ends.
3. The surfaces of the tube samples and the end caps were cleaned by sanding followed by grease removing and acetone wiping.
4. Appropriate amount of Scotch-Weld (2216 B/A Grey Epoxy Adhesive) was prepared by mixing 70 gr of modified amine (accelerator) and 50 gr of modified epoxy (base).
5. The adhesive was applied on the surface of the end caps, on the inner surface of the tube and across the tube cross section as shown in Fig. 3a.
6. The end caps were attached at the one end of the tube first. The bonded side was then positioned at the bottom so that any extensive adhesive leakage is prevented.
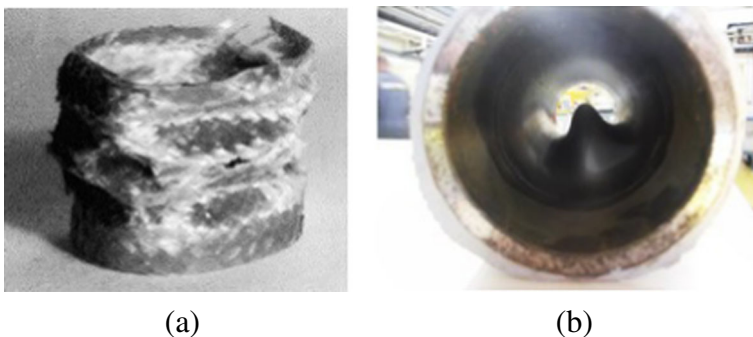


(a)                                                              (b)

**Fig. 2** Difference in axial and lateral buckling **a** Axial buckling of glass/PP composite tube [36] **b** lateral buckling of a steel/composite hybrid cylinder [37]

7.  Same procedure was performed for all the tubes. The adhesive was left to cure under two heating lambs overnight while the tubes and end caps were clamped in order to achieve better adhesion as shown in Fig. 3b.
8.  The same procedure was followed for the adhesion of the end caps at the other end of the tubes.
9.  Once both end caps were fitted and the adhesive was semi-cured, all tubes were left overnight in an oven at 60 °C for the adhesive to fully cure, according to the recommendations of the adhesive supplier.

This study focused on the hydrostatic testing of tubes to failure. The tubes were tested in a pressure pot with capacity of 6 litres which can reach testing pressures equal to 1,973 bars. The testing equipment consists of a piston, pressure transducers, a pressure pot and a tube which is used in order to pump in water to the pressure pot. The test specimen is placed inside the pressure pot, water is pumped in and any rapid change in the pressure is translated as failure as water starts coming through the crushed specimen. This change in the pressure is detected by the pressure transducers. The pressure pot operates at a controlled temperature. The test follows an ASTM D2736-78 standard testing procedure. Approximately three to four tubes per configuration were tested to failure and the average performance is presented in the next section.
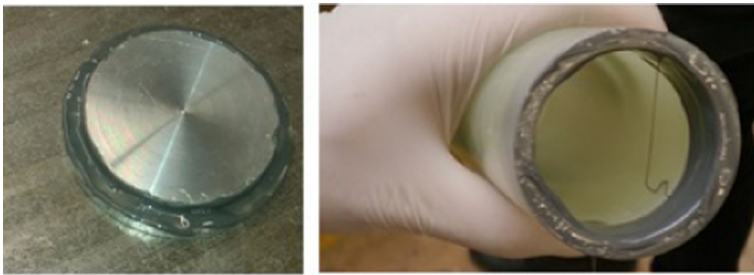


(a) End cap bonding process for the specimen preparation.
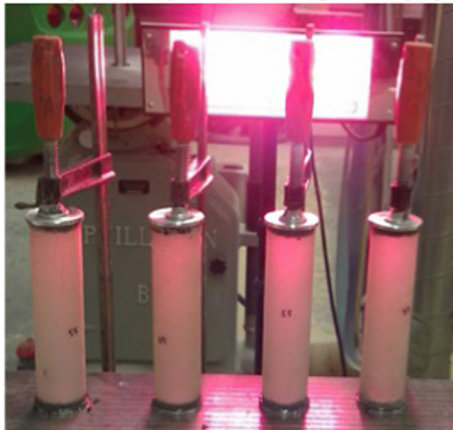


(b) Tubes clamped and under heating lamp for the pre-cure of the adhesive.

**Fig. 3**   Specimen preparation

# 5  Results

## 5.1  Pre-Preg Tubes

For the manufacturing of the laminated tubes, two types of fabrics were considered. Both types were reinforced with glass fibres; the standard property tubes are made of plain weave while the enhanced property black and clear as standard are made of 4-harness satin weave. Both plain weave (style 7637) and 4-harness satin weave were reinforced with E-glass fibres, impregnated with epoxy resin, with a total fibre volume of 60 % as shown in Fig. 4. Plain weave indicates the most simple textile weave style where the weft alternates over and under the warp. In contrast, in the 4-satin weave, the fill yarn passes over three warp yarns and under one. The difference in the weave style has an imminent impact on the fibre volume fraction along the two main directions.

The thickness of each ply was 0.23 mm for the plain weave and 0.25 for the 4-harness satin weave. The respective mechanical properties are illustrated in Table 1 as provided by the tube supplier. The tubes were wound at 0/90 degrees; the weft direction was aligned with the axial axis of the tube and the warp direction was aligned with the circumferential direction of the tube. The length of all the manufactured tubes was 220 mm length and their internal diameter was 50 mm. Tubes were made at a range of wall thicknesses from 2 mm to 5 mm. (Fig. 4). As shown in Table 1 the axial and hoop tensile and compressive strength of the 4-harness satin weave are directly related to the fibre reinforcement pattern. As a result the axial strengths are more than 4 times lower than the respective hoop strengths.

The tubes were cut to size and the specimens were appropriately prepared for testing in the pressure pot under hydrostatic compression as described in Section 4. Figure 5 illustrates representative examples of failed tubes made of plain weave and 4-harness satin weave. As shown, failure initiated at the centre of the tube across its length due to fibre cracking and delamination and further propagated towards the end caps. The primary observation is that the tubes failed due to a combination of inelastic buckling and axisymmetric yield failure. Satin weave exhibited a more brittle failure compared to plain weave which is probably
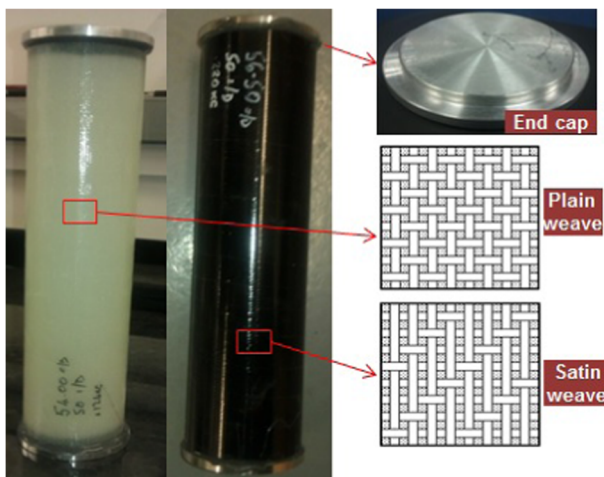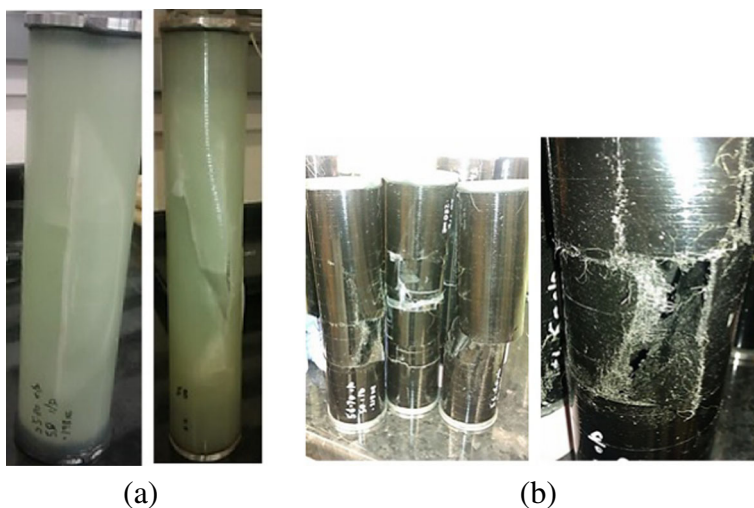


**Fig. 4**  Illustration of specimens with fitted end caps prior to testing

**Table 1** Material properties for plain weave and 4-harness satin weave E-glass fabric impregnated with epoxy resin

| Mechanical properties | Plain weave | 4-harness satin weave |
|---|---|---|
| Young's modulus (Hoop): $E_1(C)$ | 20 GPa | 35 MPa |
| Young's modulus (Axial): $E_2(C)$ | 20 GPa | 8.9 GPa |
| Shear strength: $G_{12}(C)$ | 3 GPa | 1.5 GPa |
| Poisson's ratio: $v_{12}(C)$ | 0.3 | 0.32 |
| Tensile strength (Hoop): $S_1(T)$ | 250 MPa | 657 MPa |
| Tensile strength (Axial): $S_2(T)$ | 250 MPa | 99 MPa |
| Compressive strength (Hoop): $S_1(C)$ | 300 MPa | 500 MPa |
| Compressive strength (Axial): $S_2(C)$ | 260 MPa | 80 MPa |

related to the fact that the satin weave consists of more fibres at the hoop direction with less fibre carrying the axial loads.

One tube from each wall thickness made out of plain weave was taken out of the batch before testing for microscopic testing. The microscopic analysis aimed to validate the porosity level through the tube thickness and hence assess the capability of the manufacturing technique. Possible porosity could mask the true failure mode. The microscopic analysis was performed on pieces machined out of the middle section of the tubes along their length, where damage due to external pressure was expected to initiate during testing. The instrument used was a Dinolite Premier2 Digital camera model number AM7013MTL with a magnification equal to 20-70x, and a resolution equal to 1280 x 960. The microscopic analysis of the plain weave tubes showed that at low wall thickness, air pockets of up to 1mm thick are present, and which could potentially act as internal delaminations that could alter the properties of the cured lamina (Fig. 6). As the tube thickness increases, the consolidation during curing is better and the number of air pockets is lower as shown in the same figure.



(a)                                         (b)

**Fig. 5** Illustration of specimens with fitted end caps after testing **a** plain weave and **b** satin weave
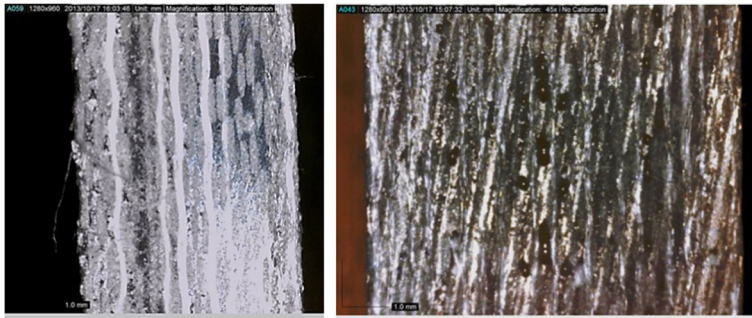
**Fig. 6** Optical microscopy results of the section of undamaged tubes illustrating through thickness air pockets after curing for a 3 mm thickness (*left*) and a 5 mm thickness (*right*) tube (Internal diameter - 50 mm)

However Fig. 7 shows an example of a specimen made of plain weave fabric of a 5 mm wall thickness and 50 mm ID, with a pre-existing macroscopic manufacturing defect. The defect was introduced during the tube lay-up when approximately 20 % of the external layers were distorted due to insufficient pre-tension. The layers with insufficient pre-tension were distorted, resulting in a 'weak point' across the tube length after curing. As shown, the defect constituted a localized lower strength, critical region from which damage initiated during hydrostatic compression.

The numerical analysis was performed with ABAQUS Version 6.12. Continuum shells (SC8R) were used in order to model the composite lay-up. The orientations of each layer of the composite lay-up were consistent with that of the experimental set-up, $[90]_n$ where $n$ represents the number of layers. This means that the model followed the experimental
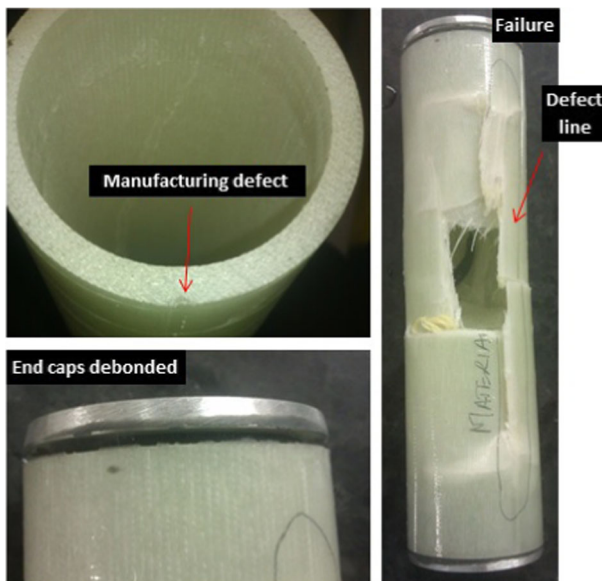


**Fig. 7** Illustration of specimens with fitted end caps and pre-introduced manufacturing defect prior and after testing

configuration where direction-1 of the fabrics was aligned with the hoop direction in order to enhance the strength of the tubes under hoop failure. The number of layers was different for each wall thickness as accurately captured during the manufacturing process of the tubes. A mesh convergence analysis identified the optimum element size which was 0.01 mm.

Initially a model with end caps was developed in order to understand the theoretical effect of the end caps on the development of stresses during external hydrostatic loads. The end caps (in this theoretical model assumed to be spherical) were modelled with solid elements (C3D8R). The spherical end caps would distribute the applied loads in a more uniform way compared to the flat end caps originally used during testing. The interphase between end caps and tube was approximated through the consideration of perfect tied contact. This was considered to be sufficient since during testing, the adhesive between the end caps and the tubes did not fail, indicating that this region was not critical. The internal diameter (ID) of the tube was 46 mm, the wall thickness (t) was 5 mm and the tube length (L) was 220 mm. Uniform external pressure equal to 12 MPa was applied on the whole model and after a static analysis, the Von Misses stresses were obtained. Results indicated that higher stress concentration occurs at the bore of the tubes while the end caps do not dictate significant physics of the problem solution. This is clearly shown in Fig. 8, where the tube-end caps interphase is not a critical region.

Figure 9 illustrates the numerical results of the developed hoop and axial stresses on the laminated tubes made of plain and 4-harness satin weave. The applied pressure was incrementally increased until failure of the tubes. The stress at failure was estimated through the maximum stress criterion according to which longitudinal and transverse failure under compressive loads occur when the stresses developed at the longitudinal ($\sigma_{11}$) and transverse ($\sigma_{22}$) directions exceed the respective strengths $S_1(C)$ and $S_2(C)$ as shown in Eqs. 7 and 8.

$$\sigma_{11} > S_1(C) \tag{7}$$

$$\sigma_{22} > S_2(C) \tag{8}$$

As observed from the properties of the two materials in Table 1, $S_1(C)$ is 500 MPa significantly higher than the respective strength of the plain weave (only 300 MPa). Since this represents the hoop reinforcement when the tubes were laminated, is it reasonable that the
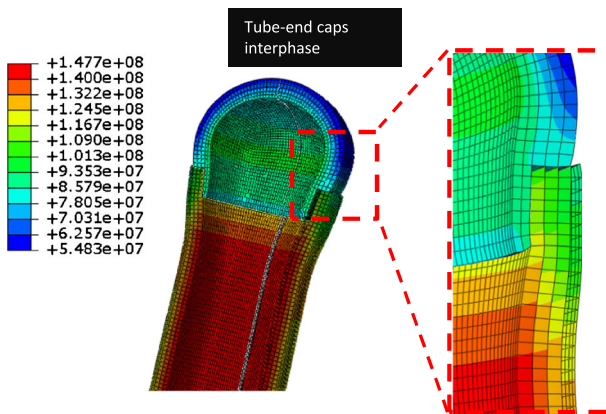


**Fig. 8** Von Misses stresses of a plain weave laminated tube (ID = 50 mm, t = 5 mm, L = 220 mm) sealed with hemispherical end caps

**Fig. 9** Compressive **a** hoop and **b** axial stresses at different applied pressures (corresponding to a water depth range equal to 3,000 - 30,000 feet) for tubes made of plain weave and 4-harness satin weave (ID = 46 mm, L = 220 mm) at a range of wall thickness (t). The maximum stress points correspond to failure as obtained from maximum stress failure criterion



(a)



(b)
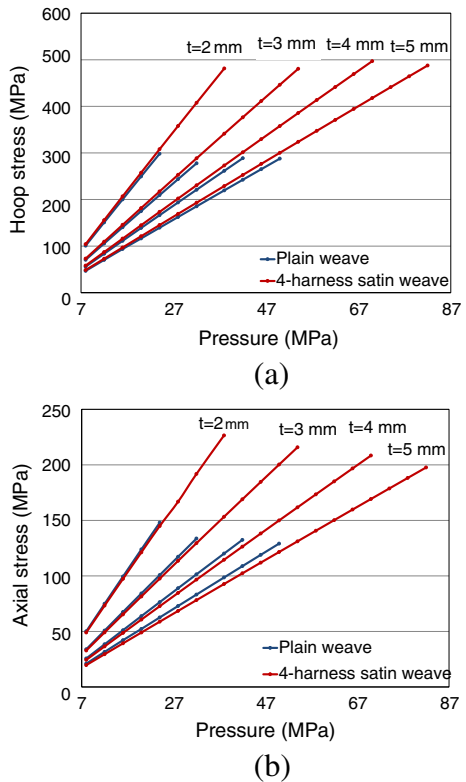
satin weave fails at much higher external pressures as shown in Fig. 9. This is also justified by the fact that the hoop stresses are two times higher than the axial stresses.

The experimental results showed the considerable advantage of the satin weave over the plain weave due to the extra reinforcement of the hoop direction. It can be observed that a superior performance can be achieved over the range of different wall thicknesses. The safe before failure water depth increases considerably with the increase in the wall thickness which would only lead to a slight increase in the tube weight.

Another method of validating the FE model was pursued through the implementation of a classical laminate theory (CLT) based analysis. ESA Comp Version 4.4.1. was used in order to calculate the resulting axial and hoop stresses of the two types of laminated tubes (plain and satin weave) under a given external pressure equal to 12 MPa. This analysis

**Fig. 10** Schematic illustration of the model employed for the calculation of the membrane forces under external pressure application in classic laminate analysis
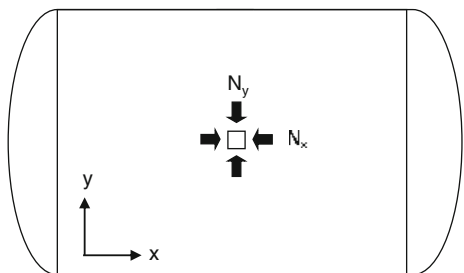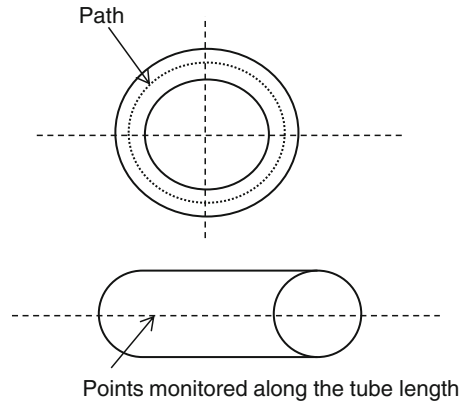
**Fig. 11** Schematic illustration of the path along which the stresses were recorded



Points monitored along the tube length

estimated the resulting stresses of a representative unit cell at the centre of the tube along its length (Fig. 10). The closed end tube was modelled as a pressure vessel where the resulting membrane forces, $N_x$ and $N_y$, per unit width and thickness at the central part of the shell, were estimated as shown in Eqs. 9 and 10.

$$N_x = \frac{1}{2} \cdot p \cdot r \tag{9}$$

$$N_y = p \cdot r \tag{10}$$

where $p$ is the applied external pressure (in this example 12 MPa) and $r$ is the tube radius.

CLT assumes that the loads are applied at the mid-plane of the laminate. Equations 9 and 10 presume a thin-walled tube. Therefore the model of the tube used for the FE preliminary analysis shown in Fig. 8, had to be redesigned in order to approximate a thin walled tube where the ratio radius/wall thickness should be higher than 10. This led to the reconfiguration of the tube external diameter (OD) to be 100 mm with a wall thickness equal to 5 mm. The tube length was kept the same (220 mm).
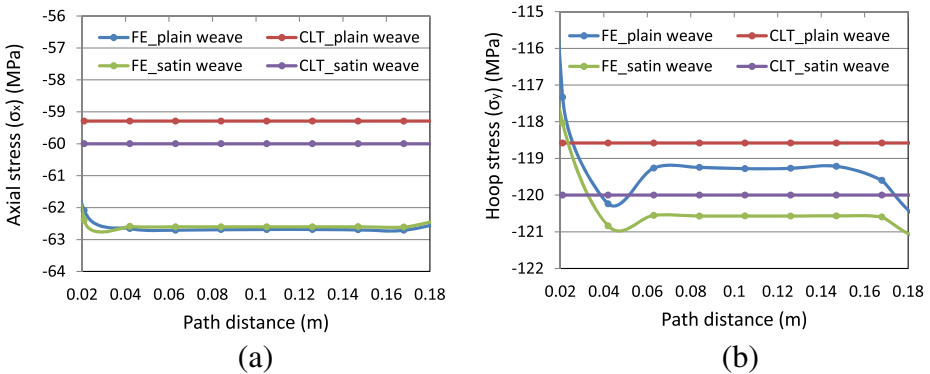


**Fig. 12** (**a**) Axial and (**b**) hoop stresses at a pressure of 12 MPa obtained from a classical laminate theory (CLT) analysis compared with numerical results for plain and satin weave over a path that corresponds to the middle layer of the laminate along the tube length (OD=100 mm, t=5 mm, L=220 mm)
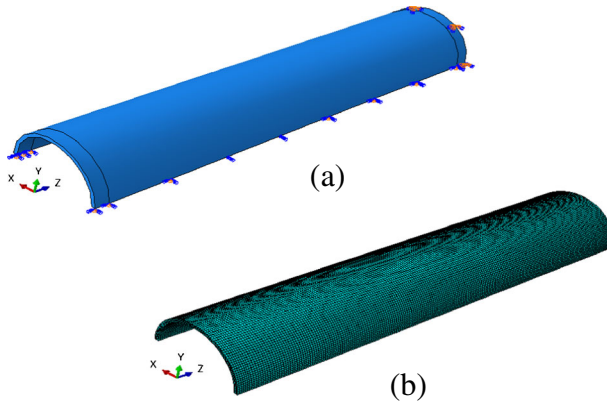
**Fig. 13** Illustration of the FE model **a** boundary conditions **b** meshed model

The FE stresses were extracted from the middle plane of the modelled tube as shown in Fig. 11. Comparison with the corresponding finite element analysis showed a significant agreement as shown in Fig. 12. It is evident that as the stress monitoring path moves towards the ends of the tube (tube-end cap interphase), the stresses obtained from the FE analysis vary due to the end effect. However this does not apply to the results obtained from classical laminate theory since the model assumes a unit cell at the centre of the tube.

Composite tubes reinforced with continuous fibres can exhibit failure due to local buckling. This crushing mode consists of the formation of local buckles. Brittle fibre-reinforced composite materials usually do not exhibit post-crushing integrity due to the lack of plastic stress-strain response and they fail in a catastrophic mode with interlaminar cracks being formed at the buckles [29]. The mechanisms that take place during such loads can be very complex to model and further interpret. For the purpose of this work, it was decided that a buckling analysis is sufficient as a good approximation in order to predict the failure loads.

Since it was proven that the end caps do not influence the performance of the tubes under external pressures, the reduction of the model size was possible, by ignoring the end caps and by applying necessary boundary conditions in order to reduce the model to half tube.
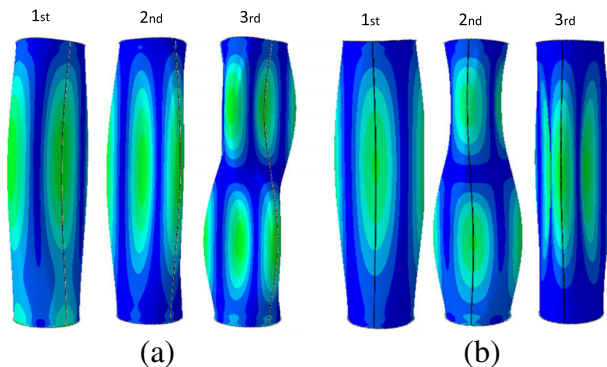


**Fig. 14** First three buckling mode shapes of laminated tubes (ID=50 mm, t=2 mm, L=220 mm) made of **a** plain weave and **b** 4-harness satin weave (deformation scale factor=1e-02)
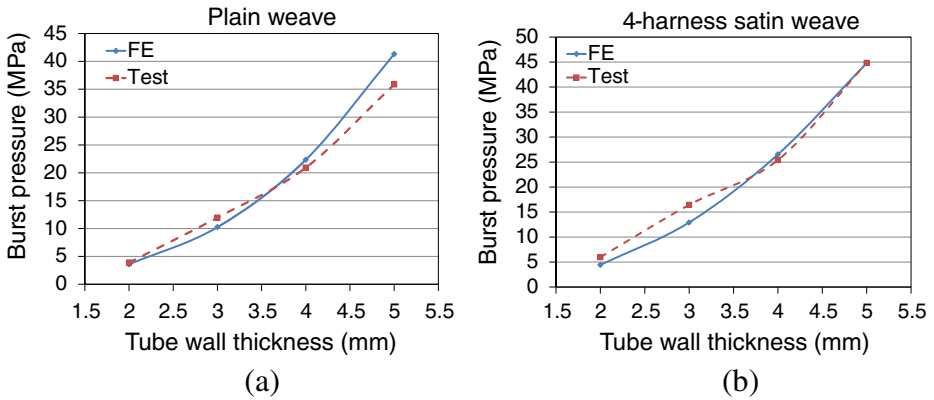
**Fig. 15** Comparison between test and numerical buckling analysis of the **a** plain and **b** satin woven laminated tubes (ID=50 mm, L=220 mm)

In addition, for the buckling analysis one end of the model was fixed and uniform pressure was applied on the external surface of the rest of the model. The boundary conditions and the meshed model are illustrated in Fig. 13.

The analysis enabled the extraction of the stresses and shapes that correspond to the buckling modes. An example of the first three buckling modes of the plain and satin weave tubes is illustrated in Fig. 14. The configuration used for this example was (ID=50 mm, t=2 mm, L=220 mm). Each material exhibited different symmetric and anti-symmetric buckling shapes. The developed FE model assumes that failure will occur between the first and the second buckling modes, where the peak stresses would develop. It should be highlighted that this modelling approach is used as a design tool in this work, while more accurate modelling should take into consideration the possible microscopic failure modes such as local buckling, delaminations and fibre fracture. These could potentially occur past the peak loads, at lower loads and until final failure.

Figure 15 illustrates a comparison between the numerical (after buckling analysis) and experimental depths at failure. A considerable agreement is achieved which indicates that
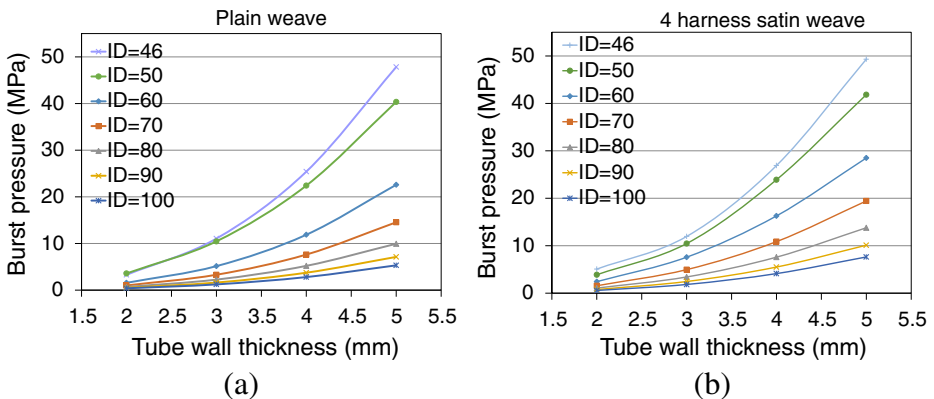


**Fig. 16** Burst pressure at a range of internal diameters (ID) and tube wall thickness for **a** plain weave and **b** satin weave laminated tubes (ID in mm)
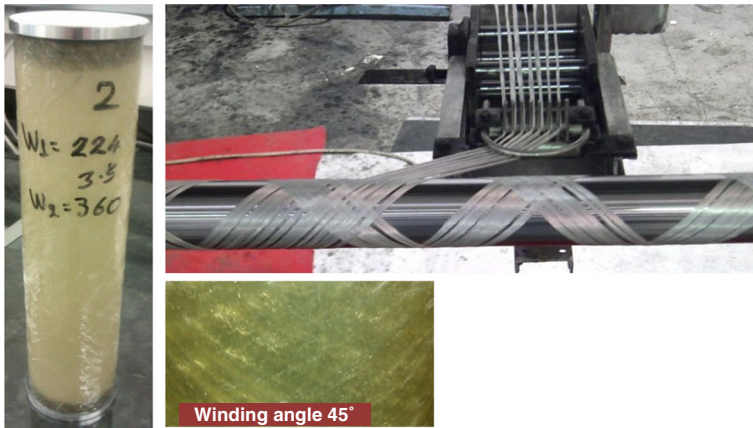
**Fig. 17** Illustration of filament wound specimens with fitted end caps prior to testing along with image taken during the fibre winding process and an example of 45° wind angle

most probably the tubes failed due to buckling. Further non destructive analysis needs to verify this assumption.

Finally the FE model was employed in order to further extend the analysis and estimate the pressure at which the tubes would fail (burst pressure) of a range of tubes configuration at various internal diameter (ID) ranging from 46 mm to 100 mm and at various wall thickness ranging from 2 mm to 5 mm. The results were based on the application of a stress failure criterion. Results show that tubes of higher ID would fail at lower pressures (hence water depths) under buckling as shown in Fig. 16.

## 5.2 Filament Wound Tubes

Filament wound tubes were manufactured at a range of wall thicknesses (2 to 4 mm) reinforced with John Manvilles 1200 tex 906 glass fibres. The manufacturing process followed the steps explained in Section 4. The resin system that was used was a urethane methacrylate Scott Blader CP1250LV resin. The analysis of the pre-preg laminated tubes showed that the optimum angle is the one closer to the hoop reinforcement. Therefore the tubes followed different winding angles, including low (45°, 55°), high (65°, 87°) as well as hybrid angles (87°/70°/87°), in an effort to investigate the effect of the angle on the performance under hydrostatic pressures.

The tubes were 220 mm long and of a 50 mm internal diameter (ID). Images of the specimens produced for testing are shown in Fig. 17. In the same figure images taken during the winding process and an example of 45° wind angle are shown. The properties of the matrix and fibres utilised for the manufacturing of the tubes are displayed in Table 2. Some

**Table 2** Material properties of the matrix and the fibres that were used for the manufacturing of the filament wound tubes

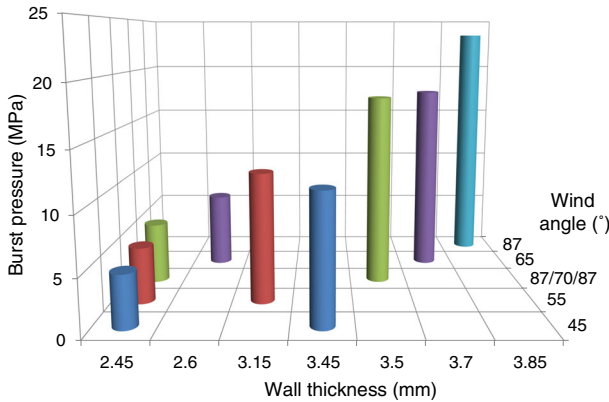| Matrix properties | $E_m$=3.28GPa | $\nu_m$=0.38 | $G_m$=1.4GPa | $\rho_m$=1,041kg/m$^3$ |
|---|---|---|---|---|
| Fibre properties | $E_f$=76 GPa | $\nu_f$=0.22 | $G_f$=26GPa | $\rho_f$=2,560kg/m$^3$ |

**Fig. 18** Burst pressure of the filament wound tubes with respect to tube wall thickness at various reinforcement angles

of these properties were given by the supplier and the rest were obtained through generic material property tables found in literature.

The tubes were tested following the test process described in Section 5. The results of the hydrostatic pressure test are illustrated in Fig. 18 where the burst pressures with respect to the tube wall thickness are plotted. As shown wind angles that approached the hoop direction ( 87° and the hybrid 87°/70°/87°) exhibited higher burst pressure. In Fig. 19 photos of the representative failed tubes are captured in an effort to illustrate the failure modes. Visual inspection of the burst tubes showed that tubes wound at high angles exhibited a more brittle behaviour as a consequence of the lack of sufficient amount of fibres to carry the axial loads, in a similar way as observed from the failure mode of the pre-preg laminated tubes.

The fibre volume fraction of the tubes, which was critical for the estimation of the material properties required for the finite element model, was unknown. It is expected that the higher the wind angle the higher the fibre volume fraction. The weight of the tubes before end cap fitting was used in order to estimate the composite density ($\rho$). This was then substituted in Eq. 11 along with the density of the matrix ($\rho_m$) and the density of the fibres ($\rho_f$), as shown in Table 2, in order to calculate the respective fibre volume fraction.
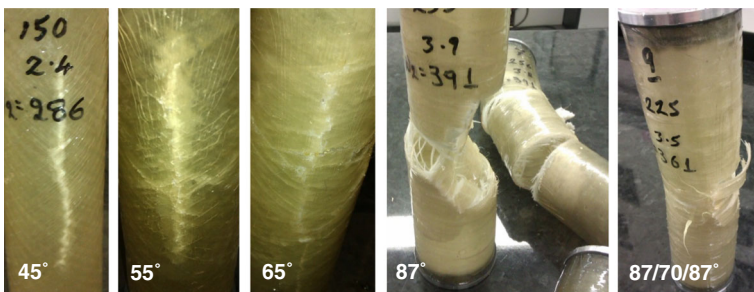
$$\rho = \rho_m \cdot (1 - f) + \rho_f \cdot f \tag{11}$$



**Fig. 19** Representative images of burst filament wound tubes of all reinforcement angles

**Table 3**  Wall thickness, density and fibre volume fraction for each wind angle

| Wind angle | Wall thickness (mm) | Density $\rho$ (kg/m$^3$) | Fibre volume fraction f (%) |
|---|---|---|---|
| 45 | 2.5 | 1,654 | 40 % |
| 55 | 2.5 | 1,654 | 40 % |
| 87/70/87 | 2.4 | 1,669 | 41 % |
| 65 | 2.6 | 1,661 | 41 % |
| 45 | 3.4 | 1,778 | 48 % |
| 55 | 3.0 | 1,839 | 52 % |
| 87/70/87 | 3.5 | 1.723 | 45 % |
| 65 | 3.7 | 1,726 | 45 % |
| 87 | 3.8 | 1,805 | 50 % |

Table 3 illustrates the estimated fibre volume fraction for each wind angle along with the density of the composite. The density and elastic properties of a unidirectional fibre reinforced ply at a specific fibre volume fraction ($f$) were calculated through the Halpin-Tsai equations. The properties were then introduced to an FE model where each filament wound layer was treated as two sub-layers of +theta and -theta fibre orientation respectively. This means if a tube with 45° fibre reinforcement and a ply thickness equal to $t$ was to be modelled, the layer in the model would consist of two sub-layers; one layer +45 angle and thickness equal to $t/2$ and another layer -45 angle and thickness equal to $t/2$.

The number of layers was determined through the number of rovings and passes needed to complete the winding until the required thickness was achieved. The simulated tubes were 220 mm long to represent the experimental set up. A buckling analysis was performed with ABAQUS Version 6.12 and the model parameters followed the same with the laminated pre-preg tubes (i.e. continuum shells SC8R, element size approximately 0.01 mm). The pressure
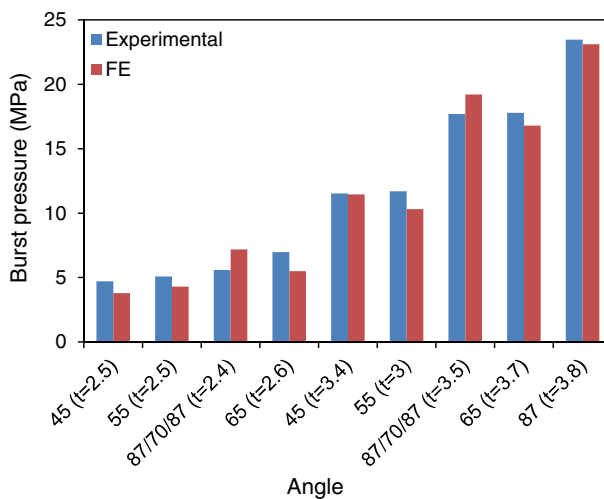


**Fig. 20**  Comparison between numerical analysis and test results of the filament wound tubes at all fibre reinforcement angles; the tube thickness (in mm) is shown in the parenthesis
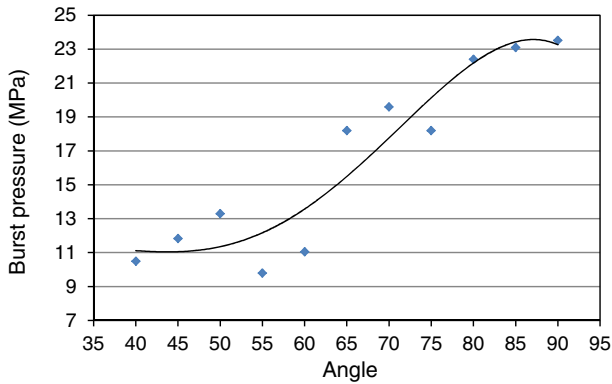
**Fig. 21** Illustration of the reinforcement angle optimisation results; burst pressure with respect to wound angle

which caused the first buckling mode was assumed to correspond to the burst pressure of the tube under external hydrostatic pressure. Figure 20 illustrates the correlation between the experimental and numerical data. X-axis illustrates the wind angle and in parenthesis the wall thickness of the tube. As shown a considerable agreement between the numerical analysis and the test results was achieved.

Figure 21 illustrates the result of the optimisation analysis in order to identify the wind angle that results in higher achievable pressures. Since this analysis was based on a hypothetical scenario and now tubes were actually made, the tube thickness was kept constant and equal to 3.5mm and the volume fraction was assumed to be 50 % for all reinforcement angles for the sake of consistency and direct comparison. In reality, the fibre volume fraction will vary depending on the wind angle, the manufacturing process, the operator/supplier and the environmental conditions control under which the tubes were manufactured. The ply thickness for this analysis was estimated from the 87 angle tubes with 50 % fibre volume fraction, as being equal to 0.3 mm (12 layers @ 3.5mm wall thickness). This simplistic study shows that as the reinforcement approaches the hoop direction the tubes will fail at
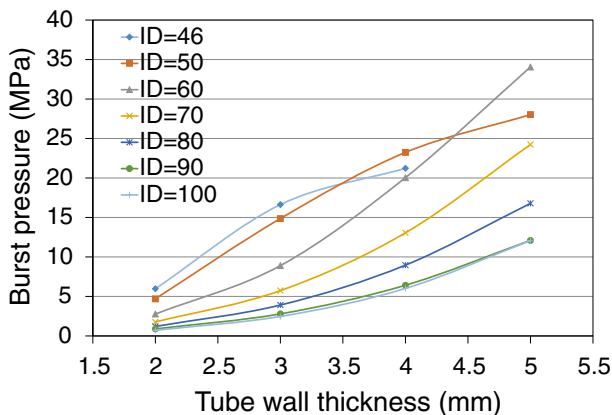


**Fig. 22** Burst pressure with respect to filament wound angle at a given fibre volume fraction (50 %), ID in mm

higher pressures and hence depths. In practice achieving a 90 degree with filament winding is difficult, therefore an angle of 87 degrees was further considered as the optimum angle for the subsequent analysis.

Finally the FE model was further extended in order to estimate the burst pressure of a range of tubes configuration at various internal diameters (ID) ranging from 46 mm to 100 mm and at various wall thickness ranging from 2mm to 5mm. Results show that tubes of higher ID would fail at lower water depths under buckling as shown in Fig. 22.

### 5.3 Braided Tubes

A 48-carrier conventional maypole braiding machine was used for the manufacturing of the braided tubes. The preforms were produced with E-glass fibres on a 600 mm epoxy resin mandrel. Three angles were produced, namely 45° with 10 layers, 55° with 8 layers and 78° with 4 layers of a thickness approximately equal to 2 mm. Epoxy resin was then injected under vacuum in order to achieve a uniform resin impregnation. The tubes were finally cut at length, equal to 220 mm (Fig. 23). All tubes were sealed with aluminium end caps which were glued with epoxy adhesive prior to testing as explained in Section 4.

The angle between the tow sets was measured using an angle devisor and the braid circumference was measured with a tape measure as accurately as possible. The measurement between the tows ($2\alpha$) as opposed to the braid angle ($\alpha$) was measured for improved accuracy and subsequently used to calculate the final braid angle. Images taken from the middle of the braid for analysis of geometrical parameters for the 45° and 80° degree fibre reinforcement are shown in Fig. 24.
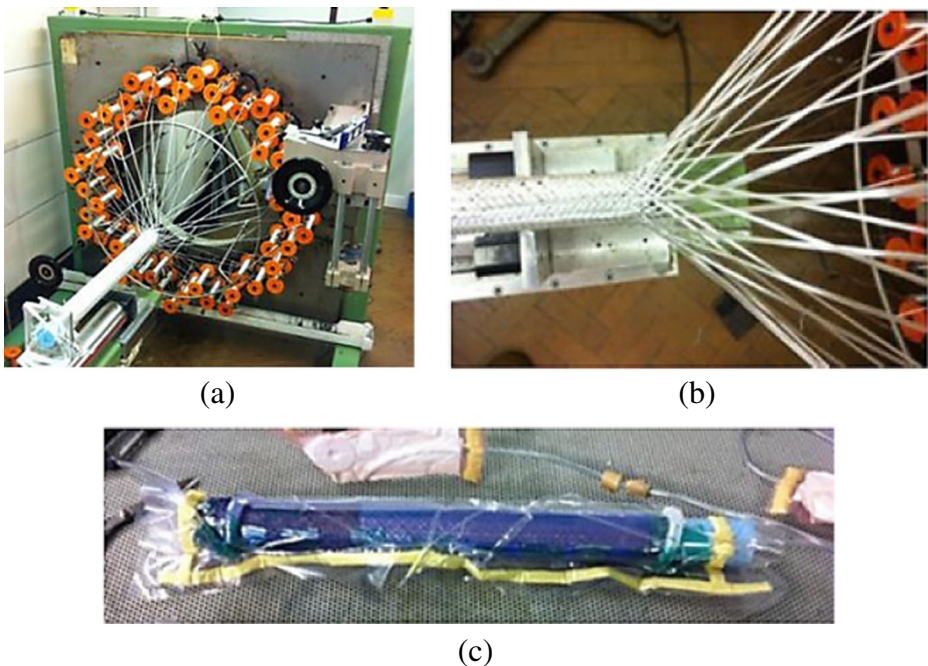


(a)                                              (b)

(c)

**Fig. 23** Fabrication of braided composite tube; **a** 48 carrier maypole braider (Cobra braiding machinery Ltd) used for braiding **b** close view of the over-braided tubular mandrel **c** vacuum assisted resin infusion

The images were then used for assessment by means of image analysis software, ImageJ. For this, an angle tool was used to map the angle between two interlacing tows in order to measure $2\alpha$. Measurements were exclusively taken from the middle of the braid (as shown by the red boxes in Fig. 24) to eliminate error caused by braid curvature and parallax. A total of 18 measurements were sampled from six images for each layer, the mean average was then calculated and assumed to be the braid angle of the respective 2D braided sheet.

The tow widths were also measured via ImageJ analysis. For tow widths a line measurement tool was used to measure the cm scale and tow widths within the images. Five measurements of 3 cm lengths were measured on the ruler and 20 tow widths sampled. The values were then converted to give the tow widths in millimetres; the mean average was taken to be the tow width for the given braid layer.

Fibre volume fraction analysis was carried out by means of matrix burn off (in accordance with ASTM D3171-99 Procedure G). The specimens were conditioned in an oven at 70°C. Specimen densities were subsequently measured through an immersion procedure before they were put into a muffle furnace at 650C for 2 hours. Fibre volume fraction and void content were calculated in accordance with calculations found in standard ASTM D3171-99 Section 14.

Both undamaged and pressure tested specimens were assessed using Scanning Electron Microscopy (SEM) in order to evaluate the resulting failure modes after testing as well as for the crimp calculation. All specimens were first cut to size using diamond and precision cutters. Undamaged specimens were additionally set in fast curing resin, ground using successively finer wet and dry rub papers before being polished using both 6 micron and 1 micron pastes. Damaged specimens were not ground.

Images of undamaged specimens were taken at a magnification of x100 and stitched together. Measurement of the tow thicknesses and crimp were sampled from stitched SEM images. The tow thickness was measured using the same methodology as that for tow width outlined above with the aid of the 200 $\mu$m scale provided. The crimp was calculated using the values of $L$ and $l$ measured from the microscopy images as shown in Fig. 25 . Table 4 outlines the geometrical characteristics of the braid.

Figure 26 shows SEM images of undamaged specimens of tubes at 45°, 55° and 78°. As observed the 45° and 55° degree specimens have more matrix rich regions than
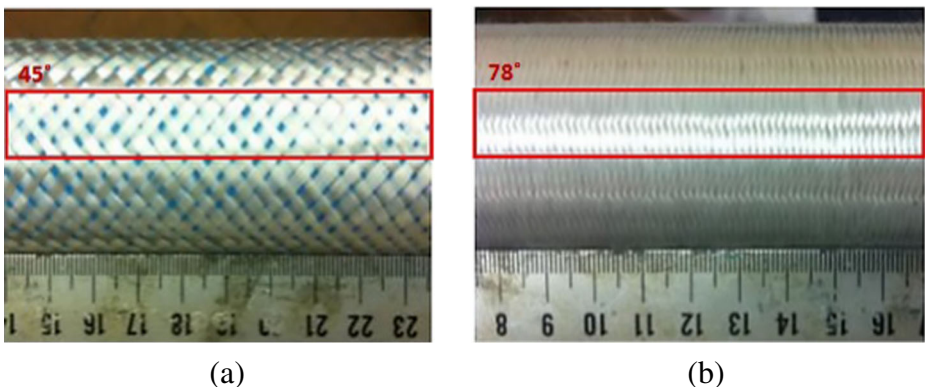


(a)                                               (b)

**Fig. 24** Images taken from the middle of the braid for analysis of geometrical parameters for **a** $\sim$ 45° and **b** 78°
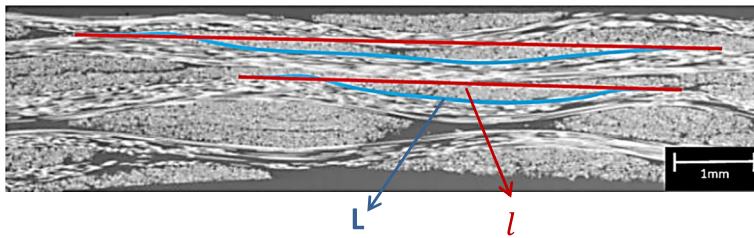
**Fig. 25** Illustration of the crimp measurements as described by (3) on an SEM image

the 78° specimen. This is also supported by the data of Table 4 where it is shown that high angles provided an increased fibre volume fraction. It is therefore suggested that at low angles the identified matrix pools are larger hence the matrix failure would be more prominent than in high angles as later verified by the test results. In addition lower angle tubes have more interlamina interfaces due to the increased number of braid layers within the structure. It is proposed that this provides a higher probability for matrix rich regions to occur due to the statistical distribution of the nesting phenomenon. These matrix rich regions are inflexible to fibre displacement and additionally provide a path of reduced resistance for crack propagation, resulting in interply failure and delamination.

The experimental burst pressure of braided tubes (Fig. 27) was compared with FE prediction. For the FE prediction of the braided tubes, a different approach needed to be followed in order to take into consideration the fibre architecture. The model followed the Byun's approach according to which the mechanical properties of the braided-textile lamina are predicted based upon the fibre and matrix properties [38]. This method utilised a transformation method of the stress/strain relations from one coordinate system to another to account for the spatially-located yards whose principal material direction does not coincide with the coordinate direction of interest. The methodology is described in detail in Byun's publication according to which the effective compliance matrix of a crimp yarn ($S$) can be

**Table 4** Summary of geometrical characteristics of the braid for each braid angle

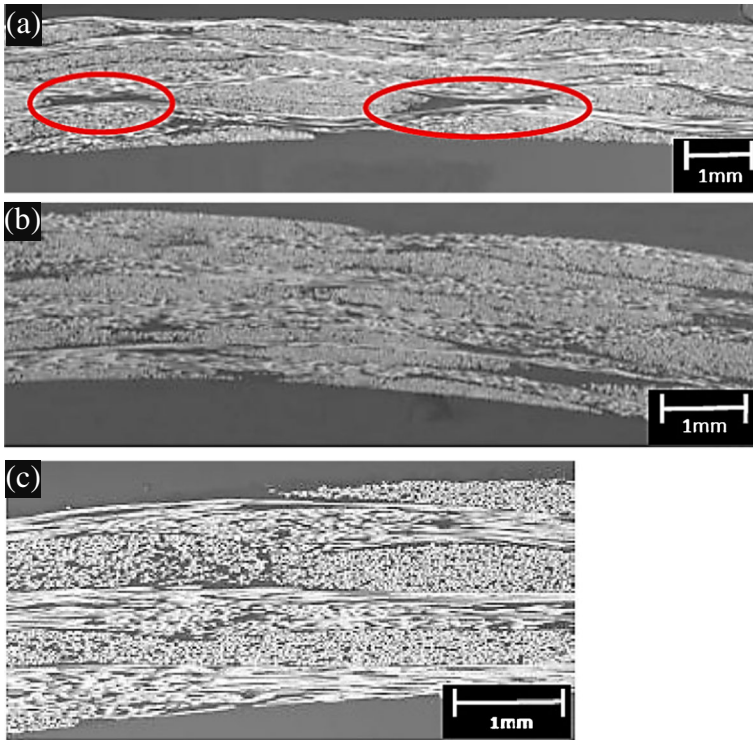|  | 45° | 55° | 78° |
|---|---|---|---|
| Fibre volume fraction (%) | 50,50 | 50,70 | 55,59 |
| Void volume (%) | 0,53 | 0,53 | 0,48 |
| Tow width (mm) | 2,56 | 3,23 | 1,75 |
| Tow thickness (mm) | 0,18 | 0,19 | 0,2 |
| Tube weight (gr) | 266 | 274 | 280 |
| Crimp (%) | 1,82 | 3,46 | 3,96 |
| Cover factor | 0,60 | 0,83 | 0,99 |
| Shrinkage factor S(%) | 1,82 | 3,46 | 3,96 |
| Crimp factor (C) | 0,018 | 0,035 | 0,041 |
| Crimp angle (degrees) | 10,95 | 15,12 | 16,18 |
| No of layers | 10 | 8 | 4 |

**Fig. 26** SEM imaging of wall cross section (parallel to tow) for; **a** 45°, **b** 55° and **c** 78°

obtained by averaging the transformed compliance matrix of the infinitesimal yarn segment through the crimp angle $\phi$ [38].

$$S_{ij}^{c} = \frac{1}{\phi} \int_{0}^{\phi'} S_{ij}' d\phi' \quad where \ (i, j = 1 - 6) \tag{12}$$
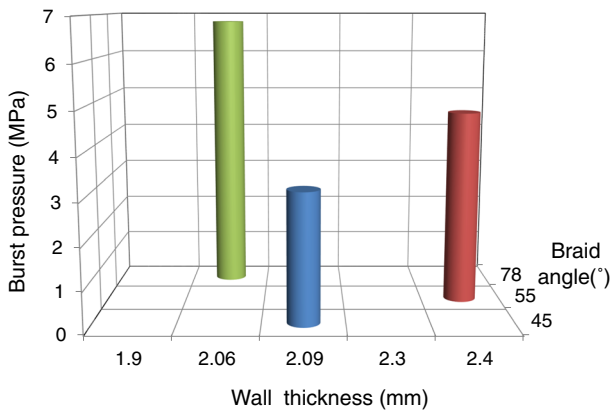


**Fig. 27** Burst pressure with respect to the tube wall thickness for the different angles of braided tubes

**Table 5** Material properties of the matrix and the fibres that were used for the manufacturing of the braided tubes

| Matrix properties | $E_m$=15. 8GPa | $\nu_m$=0.38 | $G_m$=5.5GPa | $\rho_m$=1,150kg/m$^3$ |
|---|---|---|---|---|
| Fibre properties | $E_f$=76 GPa | $\nu_f$=0.22 | $G_f$=31.3GPa | $\rho_f$=2,560kg/m$^3$ |

The high level steps that the method follows are:

1. Calculation of the in plane engineering constants through the rule of mixture, where the inputs needed were: fibre volume fraction (Table 4), fibre and matrix properties as obtained from the materials supplier (Table 5).
2. Formulation of the compliance matrix [S] in the 1-2-3 coordinate systems (Fig. 28).
3. Formulation of the effective compliance [$S^c$] matrix of a crimp yarn in the x'-y-x co-ordinate system, where inputs needed were the crimp angle $\phi$.
4. Formulation of the effective compliance matrix [$S^b$] in the x-y-z co-ordinate system. For this step the braided lamina was considered to be made of two sub-layers of half the lamina thickness with + and – the orientation angle (e.g. ±45, ±55 and ±78).
5. Formulation of the effective stiffness $C^{ij}$ of the composite, where the compliance of axial and braider yarns is inverted to stiffness, and then they are averaged over the unit cell volume.

$$C_{ij}^c = C_{ij}^a \frac{V_a}{V_t} + C_{ij}^{bp} \frac{V_b}{2V_t} + C_{ij}^{bm} \frac{V_b}{2V_t} + C_m(1 - V_y) \tag{13}$$

where (i,j=1-6), $C^a$, $C^{bp}$, $C^{bm}$ and $C^m$ are the inverted stiffness of axial, braider yarns of $\pm\theta$ orientations and matrix respectively. $V_a$ and $V_b$ are the volumes of axial and braider yarns respectively. $V_y$ is the yarn volume fraction while $V_t$ is the total volume.

**Fig. 28** Coordinate systems of a crimp yarn employed in the current work for the calculation of the braided lamina engineering constants (original figure in [38])
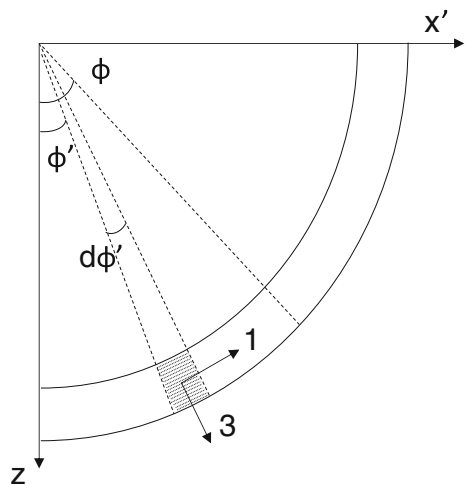
6.  Formulation of the inverted of the $C^{ij}$ matrix to the compliance $S^{ij}$.
7.  Calculation of the engineering constants of the braided textile lamina as:

$$E_{xx} = \frac{1}{S_{11}^c}; \quad E_{yy} = \frac{1}{S_{22}^c}; \quad E_{zz} = \frac{1}{S_{33}^c};$$

$$G_{yz} = \frac{1}{S_{44}^c}; \quad G_{xz} = \frac{1}{S_{55}^c}; \quad G_{xy} = \frac{1}{S_{66}^c};$$

$$\nu_{xy} = -\frac{S_{12}^c}{S_{11}^c}; \quad \nu_{zx} = -\frac{S_{13}^c}{S_{33}^c}; \quad \nu_{yz} = -\frac{S_{23}^c}{S_{22}^c} \tag{14}$$

The resulting lamina properties as calculated with the aforementioned approach were then directly imported to the ABAQUS model for buckling analysis that followed the same method that was performed for the laminated and filament wound tubes. Figure 29 displays the FE predicted burst pressure of the first buckling mode for the tubes of all considered braid angles compared with the resulting hydrostatic test burst pressures. As shown the employed FE approach for the prediction of the theoretical burst pressure of the braided tubes is more accurate for low braid angles while for the high angles the theoretical and experimental results show higher disagreement. The poor agreement between the predicted and experimental burst pressure possibly means that at high angles which exhibit higher compressive strength, the tube does not fail at the peak pressure and the fibres continue carrying loads of a lower magnitude while the cracks propagate until the final fracture of the tube. As a result the FE model underestimates the load the tubes can withstand prior to failure since it assumes that the tubes will fail at the peak pressure.

Visual inspection of the experimentally tested tubes, showed that all tubes exhibited catastrophic failure approximately central to their length. Stresses at the centre of the tubes are anticipated to be larger than areas at either end due to the reinforcing effects of the end caps.

The sign of hoop and axial stress on fibre composites can be observed from the failure modes of the braided composite tubes. With the change in tube fibre orientation, the direction of the propagating stresses on the fibre varies. A hoop stress dominated failure was
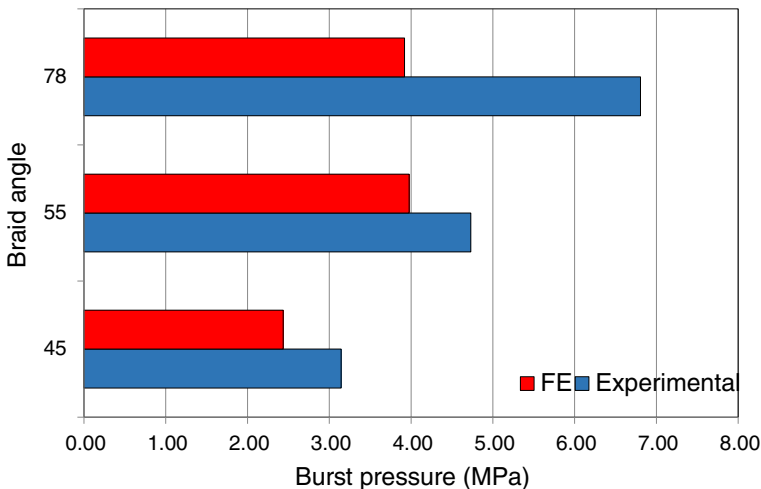


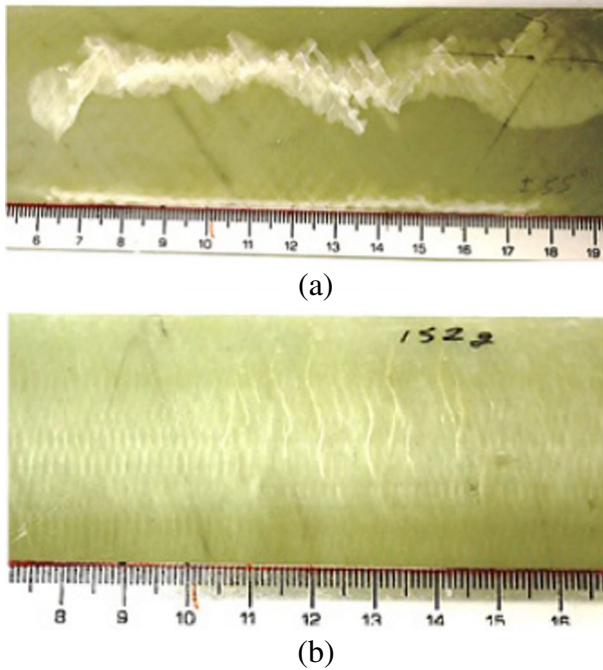**Fig. 29** Comparison between numerical analysis and test results for the braided tubes

(a)



(b)

**Fig. 30** Example images to present the appearance of failure at peak pressure **a** 45° and **b** 78°

prominent on the low angle ($\leq$ 55°) braided composite tube. The main failure mode was cracks running along the length of the tube for 55° reinforcement as shown in Fig. 30a. Composite tubes with fibres oriented towards the hoop direction had axial load dominated failure mode. As the braid structures were biaxial, there were no axial fibres to withstand the load in the axial loading direction. The axial load was acting transverse to the fibre orientation. Matrix cracks appearing in the direction of the fibre (at 78°) indicate the sign of axial loading in the failure of the tube as shown in Fig. 30b.

Significant delamination occurred in all low angle specimens, especially that of 45° as a result of the resin rich pockets. Figure 31 illustrates the delamination which occurred within the region of catastrophic failure and within the region closer to the end caps. It may be seen here that delamination is concentrated between two layers rather than distributed between
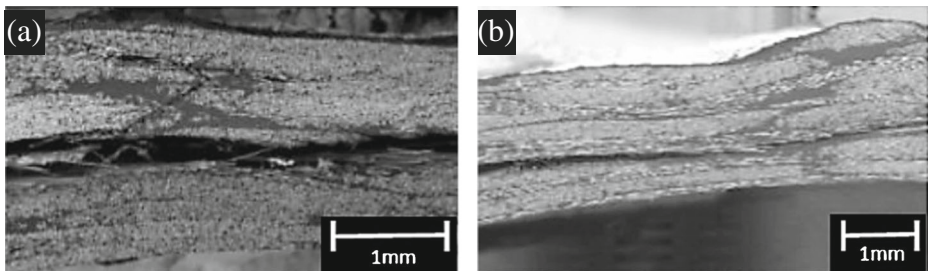


**Fig. 31** Delamination failure at peak pressure of 45° at **a** central along the length of the tube and **b** close to the end cap
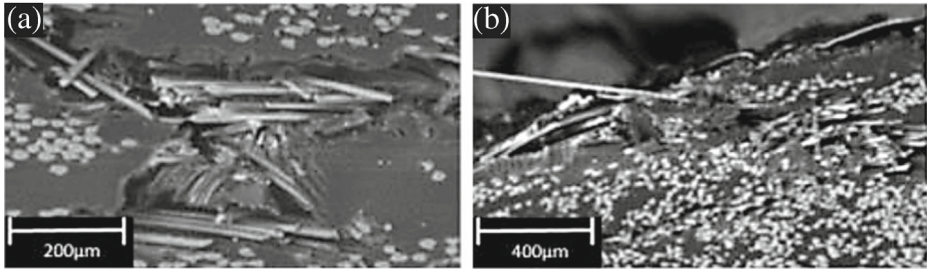
**Fig. 32** Evidence of fibre fracture at peak pressure; **a** 45° centre of wall at point of failure, **b** 45° outer surface of wall at point of failure

multiple suggesting that it is likely that delamination throughout the sample will tend to remain between two specific braid layers.

Figure 32 illustrates the fibre fracture observed via SEM of the catastrophic failure point of 45°. Fibre fracture only occurred in specimens identified to exhibit delamination and visa versa which indicates that the two failure modes are related. It is considered that matrix failure and delamination about displaced reinforcement provides scope for further fibre movement. This is because failure of the matrix results in reduced reinforcement support, resulting in fibre fracture. Fibre fracture occurred in both the low angle and 78° specimens.

Figure 33 illustrates a 55° tube where, like other specimens observed, crack propagation follows along heavily fibre occupied regions. Here interface failure occurs as well as matrix failure at points between closely positioned fibres. This shows that the fibre-matrix interface is weak relative to the matrix resulting in failure of the latter.

Figure 34 illustrates the orientation of fracture along 78° and 55° tubes. The nature of crack propagation naturally follows the orientation of the two as this is more energetically favourable (fibres are stronger therefore take more energy to break than the matrix). Failure is being diverted upon meeting an interlacement, hence "arresting" the propagating crack. It is proposed that the redirection of crack orientation is a result of the support provided by the increased tow packing (tow density) of the high angle braids. For low angles, the lack of tow packing provides matrix rich regions at the centre of the unit cell which does not provide sufficient crack arrest capability at the points of interlacement. Therefore, the crack propagation is much less controlled. It is anticipated that the increase in crack arrest
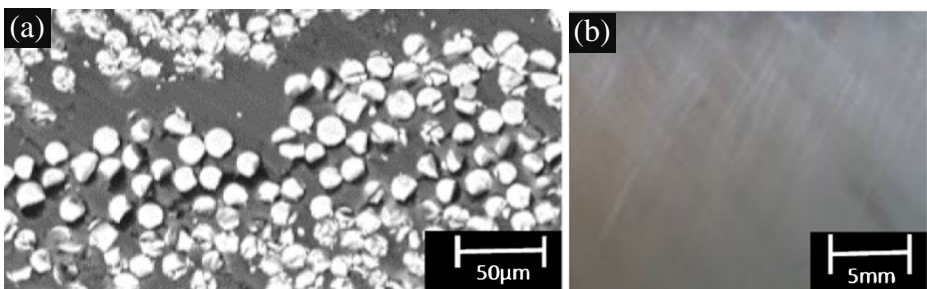


**Fig. 33** Evidence of interface failure at peak pressure; **a** microscopic view of tow cross section (SEM specimen was ground) and **b** view of outer surface of shell wall
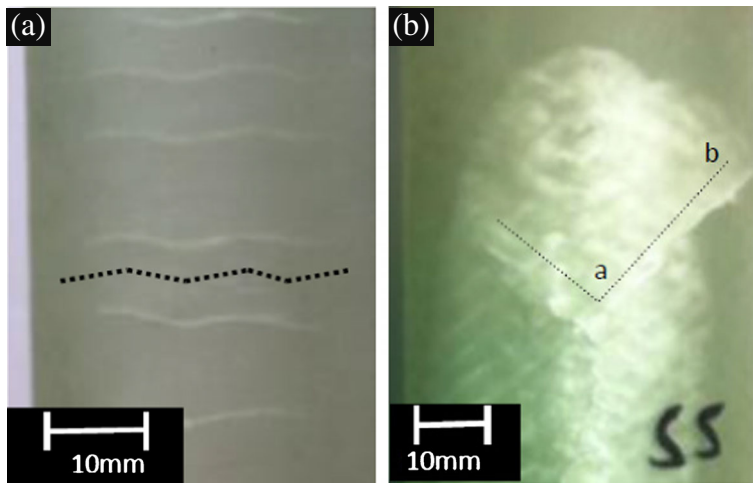
**Fig. 34** Fracture along **a** 78° tube and **b** 55° tube at peak pressure

capabilities is one of the contributing factors to the overall improved performance of the high angle specimens.

## 6 Concluding Remarks

This work studied the performance of composite tubes when subjected to external hydrostatic pressures. First a literature review highlighted the most critical design and manufacturing parameters for textile composite tubes; filament wound and braided. Then the work focused on the experimental and numerical analysis of pre-preg laminated tubes made of plain and satin weave and filament wound and braided tubes wound at a range of reinforcement angles. Their corresponding behaviour under external hydrostatic pressure was investigated. Finite element (FE) models of the tubes were generated in order to investigate the theoretical performance of a bigger range of tube thickness and internal diameters compared to what was tested. The FE analysis assumed that buckling is the primary cause of failure and hence focused on the study of the pressures causing the tube buckling modes. Classic laminate theory was conducted through ESA Comp software in order to further validate the FE models generated specifically for the laminated tubes. Then the same FE modelling approach was followed for filament wound tubes manufactured at a range of winding angles in order to establish which is the most optimum angle. This part followed a simple approach of estimating the material carts required for the FE simulation based on the Halpin-Tsai equations for the filament wound tubes and on a modified model proposed previously in literature for the braided tubes. The FE prediction of the braided tubes performance was based on a modified model according to which the effective compliance matrix of a crimp yarn can be obtained by averaging the transformed compliance matrix of the infinitesimal yarn segment through the crimp angle. The FE models were developed and successfully validated against the test results. An optimisation study was conducted for the filament wound tubes which indicated that the optimum angles for maximum resistance

against external hydrostatic pressures are the ones closer to the direction of the hoop reinforcement. Finally SEM was conducted for the braided tubes in order to further understand the failure modes from a microscopic aspect.

The work concluded that the failure mechanisms of composite tubes when exposed to external hydrostatic pressures are complex and therefore design against external pressures needs careful consideration. As SEM images of the braided tubes showed, the failure mode is mixed, potentially affecting the fibres, matrix as well as the interphase. In addition, the FE analysis of non conventional fibre reinforced tubes such as filament wound and braided is not always straightforward. This study followed simple approaches which focused on the establishment of layer-by-layer lay-up built. However to obtain the material properties of a single layer when the fibre reinforcement consists of interlacements can be challenging. This study demonstrated a simplified modelling approach which was successfully validated against the test results. Furthermore it can be argued that although the different manufacturing methods can not be directly compared, the filament wound and braided tubes can potentially exhibit higher resistance to external hydrostatic pressure compared to the pre-preg laminated tubes. Finally, the study proved that although previous work suggests that fibre reinforcement of 55° offers the highest resistance to internal pressure, the same principle does not apply for external pressure, where the tubes with fibre reinforcement approaching the hoop direction exhibiting higher performance. This lies on the fact that the distribution of axial and transverse loads during application of internal pressure is different to the application of external pressure hence leading to different failure mechanisms. External pressure results in higher forces being applied on the hoop direction compared to axial, while internal pressure results in a different load distribution where axial and hoop fibres both contribute significantly to the tube burst strength.

# References

1. Li, Z.M., Shen, H.S.: Postbuckling of 3d braided composite cylindrical shells under combined external pressure and axial compression in thermal environments. Int. J. Mech. Sci. **50**(4), 719–731 (2008)
2. Ayranci, C., Carey, J.: 2d braided composites: a review for stiffness critical applications. Composite Structures **85**(1), 43–58 (2008)
3. Potluri, P., Manan, A., Francke, M., Day, R.: Flexural and torsional behaviour of biaxial and triaxial braided composite structures. Compos. Struct. **75**(14), 377–386 (2006)
4. Potluri, P., Rawal, A., Rivaldi, M., Porat, I.: Geometrical modelling and control of a triaxial braiding machine for producing 3d preforms. Compos. A: Appl. Sci. Manuf. **34**(6), 481–492 (2003)
5. Karbhari, V.M., Falzon, P.J., Herzberg, I.: Energy absorption characteristics of hybrid braided composite tubes. J. Compos. Mater. **31**(12), 1164–1186 (1997)
6. Chiu, C.H., Tsai, K.H., Huang, W.J.: Effects of braiding parameters on energy absorption capability of triaxially braided composite tubes. J. Compos. Mater. **32**(21), 1964–1983 (1998)
7. Chiu, C., Tsai, K.H., Huang, W.: Crush-failure modes of 2d triaxially braided hybrid composite tubes. Compos. Sci. Technol. **59**(11), 1713–1723 (1999)
8. Rosenow, M.: Wind angle effects in glass fibre-reinforced polyester filament wound pipes. Composites **15**(2), 144–152 (1984)

9. Soden, P., Kitching, R., Tse, P., Tsavalas, Y., Hinton, M.: Influence of winding angle on the strength and deformation of filament-wound composite tubes subjected to uniaxial and biaxial loads. Compos. Sci. Technol. **46**(4), 363–378 (1993)
10. Mertiny, P., Ellyin, F.: Influence of the filament winding tension on physical and mechanical properties of reinforced composites. Compos. A: Appl. Sci. Manuf. **33**(12), 1615–1622 (2002)
11. Cohen, D.: Influence of filament winding parameters on composite vessel quality and strength. Compos. A: Appl. Sci. Manuf. **28**(12), 1035–1047 (1997)
12. Lea, R.H., Yang, C.: Improving the Mechanical Properties of Composite Pipe Using Multi-Angle Filament Winding. Tech. Rep., NACE International, Houston, TX (United States) (1998)
13. Mertiny, P., Ellyin, F., Hothan, A.: Stacking sequence effect of multiangle filament wound tubular composite structures. J. Compos. Mater. **38**(13), 1095–1113 (2004)
14. Potluri, P., Nicolais, L.: Braiding, John Wiley & Sons Inc. (2011)
15. Douglas, W.: Braiding and braiding machinery, Centrex publishing company; Cleaver-Hume press (1964)
16. Rawal, A., Potluri, P.: Geometrical modeling of the yarn paths in three-dimensional braided structures. J. Ind. Text. **35**(2), 115–135 (2005)
17. Byun, J., Chou, T.: Modelling and characterization of textile structural composites: a review. The Journal of Strain Analysis for Engineering Design **24**(4), 253–262 (1989)
18. Tate, J.S., Kelkar, A.D., Whitcomb, J.D.: Effect of braid angle on fatigue performance of biaxial braided composites. Int. J. Fatigue **28**(10), 1239–1247 (2006). The Third International Conference on Fatigue of Composites The Third International Conference on Fatigue of Composites
19. Naik, R.A., Ifju, P.G., Masters, J.E.: Effect of fiber architecture parameters on deformation fields and elastic moduli of 2-d braided composites. J. Compos. Mater. **28**(7), 656–681 (1994)
20. Hull, D.: A unified approach to progressive crushing of fibre-reinforced composite tubes. Compos. Sci. Technol. **40**(4), 377–421 (1991)
21. Inai, R., Chirwa, E., Saito, H., Uozumi, T., Nakai, A., Hamada, H.: Experimental investigation on the crushing properties of carbon fibre braided composite tubes. International Journal of Crashworthiness **8**(5), 513–521 (2003)
22. Karbhari, V., Haller, J.: Rate and architecture effects on progressive crush of braided tubes. Compos. Struct. **43**(2), 93–108 (1998)
23. Harte, A.M., Fleck, N.A.: On the mechanics of braided composites in tension. European Journal of Mechanics - A/Solids **19**(2), 259–275 (2000)
24. Hull, D., Clyne, T.: An introduction to composite materials. Cambridge Solid State Science Series Cambridge University Press (1996)
25. Hull, D., Legg, M., Spencer, B.: Failure of glass/polyester filament wound pipe. Composites **9**(1), 17–24 (1978)
26. Xia, M., Takayanagi, H., Kemmochi, K.: Analysis of multi-layered filament-wound composite pipes under internal pressure. Compos. Struct. **53**(4), 483–491 (2001)
27. Srikanth, L., Rao, R.: Strength and stiffness behaviour of braided and filament wound glass epoxy composites simultaneous studies and comparison. J. Compos. Mater. **48**(4), 407–414 (2014)
28. Mistry, J., Gibson, A., Wu, Y.S.: Failure of composite cylinders under combined external pressure and axial loading. Compos. Struct. **22**(4), 193–200 (1992)
29. Farley, G.L., Jones, R.M.: Crushing characteristics of continuous fiber-reinforced composite tubes. J. Compos. Mater. **26**(1), 37–50 (1992)
30. Gning, P., Tarfaoui, M., Collombet, F., Riou, L., Davies, P.: Damage development in thick composite tubes under impact loading and influence on implosion pressure: experimental observations. Composites Part B: Engineering **36**(4), 306–318 (2005)
31. Mistry, J.: Theoretical investigation into the effect of the winding angle of the fibres on the strength of filament wound {GRP} pipes subjected to combined external pressure and axial compression. Compos. Struct. **20**(2), 83–90 (1992)
32. Messager, T., Pyrz, M., Gineste, B., Chauchot, P.: Optimal laminations of thin underwater composite cylindrical vessels. Compos. Struct. **58**(4), 529–537 (2002)
33. Olivas, J.D., Ravi-Chandar, K., Bustillos, J., Craigie, L.: Buckling of filament-wound cylindrical vessels subjected to external pressure. J. Pressure Vessel Technol. **118**(2), 216–220 (1996)
34. Satheesh, P., Kumar Reddy, C., Krishna, T.: Optimum design and analysis of filament wound composite tubes in pure and combined loading. International Journal of Engineering Research & Technology **1**(8) (2012)
35. Smith, P., Ross, C., Little, A.: Collapse of composite tubes under uniform external hydrostatic pressure. In: 7th International Conference on Modern Practice in Stress and Vibration Analysis, Journal of Physics: Conference Series, vol. 181 (2009)

36. Harte, A.H., Fleck, N.: Deformation and failure mechanisms of braided composite tubes in compression and torsion. Acta Mater. **48**(6), 1259–1271 (2000)
37. Davies, P., Bigourdan, B., Chauchot, P.: Composite cylinders for deep sea applications: an overview. ASME. J. Pressure Vessel Technol. **138**(6), 060,907–060,907–8 (2016)
38. Byun, J.H.: The analytical characterization of 2-d braided textile composites. Compos. Sci. Technol. **60**(5), 705–716 (2000)